Structural and band tail state photoluminescence properties of amorphous SiC films with different amounts of carbon*

Fu Guang-Sheng(傅广生), Wang Xin-Zhan(王新占)†, Lu Wan-Bing(路万兵), Dai Wan-Lei(戴万雷), Li Xing-Kuo(李兴阔), and Yu Wei(于 威)

College of Physics Science and Technology, Hebei University, Baoding 071002*, China*

(Received 21 March 2012; revised manuscript received 8 May 2012)

Amorphous silicon carbide films are deposited by the plasma enhanced chemical vapour deposition technique, and optical emissions from the near-infrared to the visible are obtained. The optical band gap of the films increases from 1.91 eV to 2.92 eV by increasing the carbon content, and the photoluminescence (PL) peak shifts from 1.51 eV to 2.16 eV. The band tail state PL mechanism is confirmed by analysing the optical band gap, PL intensity, the Stocks shift of the PL, and the Urbach energy of the film. The PL decay times of the samples are in the nanosecond scale, and the dependence of the PL lifetime on the emission energy also supports that the optical emission is related to the radiative recombination in the band tail state.

Keywords: amorphous silicon carbide, band tail state photoluminescence, time-resolved photoluminescence

PACS: 78.66.Jg, 78.55.–m, 78.47.jd **DOI:** 10.1088/1674-1056/21/10/107802

1. Introduction

Due to the property of bandgap adjustability, hydrogenated amorphous silicon carbide (α-SiC:H) has great potential application in optical emission adjustable light emitting diodes, diluted magnetic semiconductors, and solar cell manufacturing.[1−4] Recently, the α-SiC:H has been fabricated by various technologies, and optical emissions from near-infrared to the visible region have been obtained. Among all the material fabrication processes, plasma enhanced chemical vapour deposition (PECVD) is considered as the technique with the most potential due to its good compatibility with the microelectronic production process.[5] The optical emission properties of α-SiC:H are greatly influenced by the growth procedures and parameters, and the PL mechanism is still not yet clear. White electroluminescence was obtained at room temperature, and the optical emission was attributed to the localized and extended states of the valence and conduction bands.[6] The PL caused by localized states of the band tail and defects of surface dangling bonds was also reported.[7] In addition, PL attributed to the quantum confinement effect of the Si nanocrystal was also obtained by Coscia *et al.*[8] The results indicate that the optical emission mechanism of α-SiC:H is complex, and it is very meaningful to obtain complementary information for a better understanding the PL mechanism of an α-SiC:H film prepared by the PECVD technique before using it in practical applications.

In this work, α-SiC:H films with different amounts of carbon are prepared by the PECVD technique, and the PL mechanism of the film is studied by absorption, steady PL, and the time-resolved PL spectrum. Analyses show that the PL originates from the SiC matrix, and all findings are well understood within the framework of the band tail PL model.

2. Experimental details

The α-SiC:H films were deposited by the PECVD technique using SiH_4, CH_4, and H_2 as reactants, and all films were deposited on single crystal silicon and corning glass substrates. The H_2 flow rate, deposition pressure, substrate temperature, deposition power, and deposition time were set at 60 standard-state

*Project supported by the National Natural Science Foundation of China (Grant No. 60878040) and the Natural Science Foundation of Hebei Province, China (Grant Nos. F2012201007 and F2012201042).

†Corresponding author. E-mail: xinzhan_wang@126.com

© 2012 Chinese Physical Society and IOP Publishing Ltd

cubic centimeter per minute (sccm), 1 Pa, 300 °C, 300 W, and 60 min, respectively. The flow rate of SiH_4 was kept at 0.6 sccm, while the flow ratios of $CH_4/(SiH_4+CH_4)$ were set to be 0.50, 0.57, 0.61, 0.69, 0.77, and 0.85, and the samples were denoted as S_1, S_2, S_3, S_4, S_5, and S_6, respectively.

The chemical compositions of the films were determined by energy dispersive X-ray analysis (EDS, Hitachi JSM-7500F). The infrared absorptions were deduced from the transmittance measurements in a Fourier transform infrared spectrophotometer (FTIR, Bio-Rad 60 V). The ultraviolet-visible (UV-VIS) absorption spectra of the samples were measured by a Zolix-SBP300 spectrometer. The steady and time-resolved PL spectra were detected by an FLS920 fluorescence spectrometer, and the exciting light sources were a 450-W Xe lamp and an EPL 375-picosecond pulsed diode laser, respectively. Curve fittings were performed on the PL decay curves to confirm the PL decay times, and all PL measurements were carried out at room temperature.

3. Results and discussion

Figure 1 shows the atom ratio C/(Si+C) versus the flow rate ratio $CH_4/(CH_4+SiH_4)$ of the film. The carbon component increases monotonically with the increase of the CH_4 flow rate, and a nearly-stoichiometric amorphous SiC:H film is obtained when the flow rate ratio $CH_4/(CH_4+SiH_4)$ is 0.77. The band gap of the α-SiC:H film can be adjusted by changing the carbon content, and the optical emission is very sensitive to the chemical composition of the film. In this way, the carbon content in the film is an important parameter for understanding the microstructure and PL mechanism of the α-SiC:H film, and the carbon content can be adjusted effectively by changing the flow ratio of CH_4 and SiH_4.

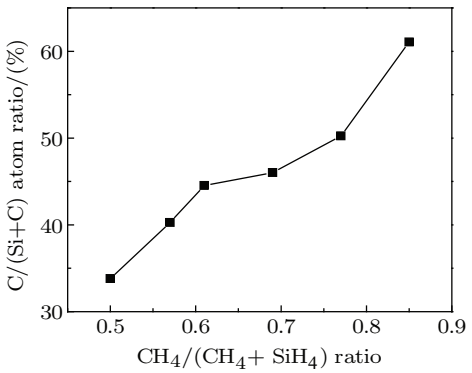


Fig. 1. Atom ratio C/(Si+C) versus flow rate ratio $CH_4/(CH_4+SiH_4)$.

Figure 2 shows the FTIR spectra of the samples at different CH_4 flow rates. Three absorption bands located at around 780, 2100, and 2900 cm^{-1} are detected, which correspond to the stretching vibration modes of Si–C, Si–H_n, and C–H_n bonds, respectively. In order to study the Si–C bond density quantitatively, Gaussian fittings are performed in a range of 500 cm^{-1}–1200 cm^{-1} by considering the contributions of C–H_n rocking/wagging vibrating modes at about 1000 cm^{-1}, Si–H_n bending modes at about 900 cm^{-1}, Si–H_n wagging or rocking modes at about 640 cm^{-1}, Si–C stretching mode at about 780 cm^{-1},[9] and the fitting result of S_5 is shown in the inset of Fig. 2.

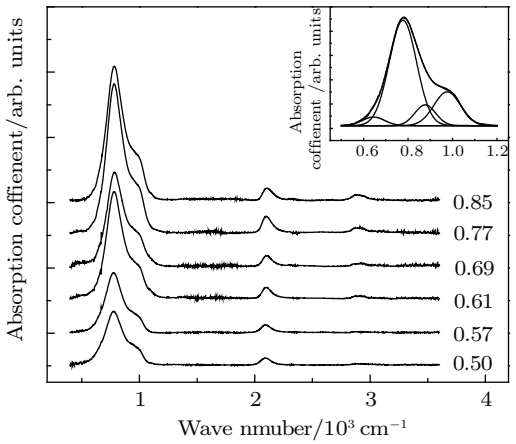


Fig. 2. The FTIR for the films with different $CH_4/(CH_4+SiH_4)$ ratios. The inset shows the curve fittings for the Si–C absorption band of S_5.

The bond density of the Si–C mode is obtained from the integrated absorption of the Si–C stretching mode, and the inverse cross section of the Si–C absorption mode is 2.13×10^{19} cm^{-2}.[10] As can be seen in Fig. 3, the bond density of the Si–C mode increases with the ratio of $CH_4/(CH_4+SiH_4)$ increasing up to 0.77, and the maximal bond density is 2.65×10^{21} cm^{-3}. The result indicates that more and more Si–C bonds form until the films change from Si-riched to C-riched. The absorption bands related to the Si–H_n stretching modes show a growing tendency with the CH_4 flow rates increasing, and the absorption peak shifts toward a higher wave number. It can be attributed to the electronegativity increasing around Si atoms when carbon atoms are introduced into the film.[11] The absorption band located at 2900 cm^{-1} corresponds to the sp^3 C–H_n (n = 1, 2, 3) stretching modes, and the bonds density increases as the carbon content increases. The sp^2 C–H_n absorption bands above 3000 cm^{-1} are not found in the spectra, which suggests that hydrogen

atoms prefer to bond to sp^3 instead of sp^2 sites of carbon, and the high H_2 dilution promotes the transformation from polymericlike $(CH_2)_n$ chains to diamondlike (sp^3 site of C–C bonding) chains by etching away the weakly bonded C–H sites and sp^2 C–C bonds.[12]

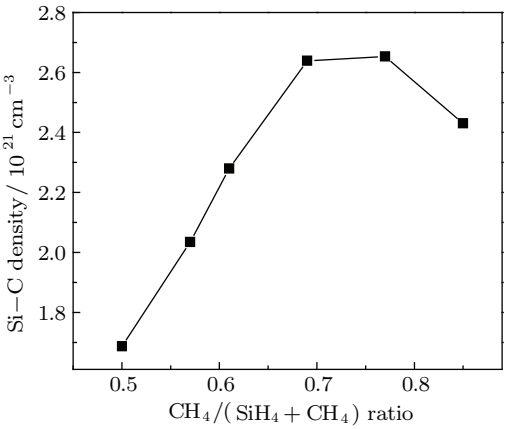


Fig. 3. The Si–C bond density of the films with different $CH_4/(CH_4+SiH_4)$ ratios.

Figure 4 shows the UV-VIS absorption spectra of the films at different CH_4 flow rates. As can be seen, the absorption edge shifts toward higher energy with the CH_4 flow rate increasing, and the optical band gap of the film can be expressed as[13]

$$\sqrt{\alpha h\nu} = B(h\nu - E_g), \tag{1}$$

where α is the absorption coefficient, $h\nu$ is the photon energy, E_g is the optical energy gap, and B is the Tauc slope (B factor). The optical band gaps can be calculated to be 1.91 eV, 2.23 eV, 2.52 eV, 2.59 eV, 2.74 eV, and 2.92 eV, respectively. This observation is consistent with the fact that the α-SiC:H films change from Si-rich to C-rich. In the Si-rich film, the bottom of the conduction band is composed of Si–Si antibonding levels, while the top of the valence band is dominated by Si–Si bonding levels.[14] The energy of the Si–C antibonding level is higher than that of Si–Si antibonding level, so the band gap increases by introducing more carbon atoms into the film. With the CH_4 flow rate further increasing, the film becomes C-riched, and the optical gap is determined mainly by Si–C and C–C bonds. The bond energy of sp^2 C–C bonding restricts the increase of the optical band gap,[15] and the continuous increase in the optical gap indicates that the excessive carbon species in the C-rich film exists as sp^3 C–C bonds, which is consistent with the FTIR spectra.

Figure 5 shows the Urbach energy (E_u) and B factor changing with the CH_4 flow rates, and the E_u is obtained as[13]

$$\alpha(E) = \exp(-E/E_u). \tag{2}$$

The E_u of the film first increases and then decreases with the increase of the CH_4 flow rate, and a maximal value is obtained in S_5, while the B factor shows an opposite tendency. It has been reported that the E_u and the B factor are related to the local and overall structural disorder in the films, respectively.[16] The opposite relationship between the E_u and the B factor indicates that local disorder leads to overall disorder. The disorder is also related to the bonding states in the film. The bond density of the Si–C mode increases until the film changes from Si-riched to C-riched, and the disorder enhancement should be caused by the differences in bond length and bond angle between Si and C atoms in the amorphous film.

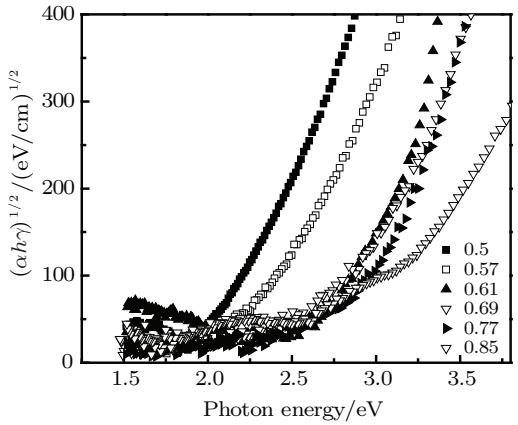


Fig. 4. Optical absorption versus photon energy for the films at different $CH_4/(CH_4+SiH_4)$ ratios.

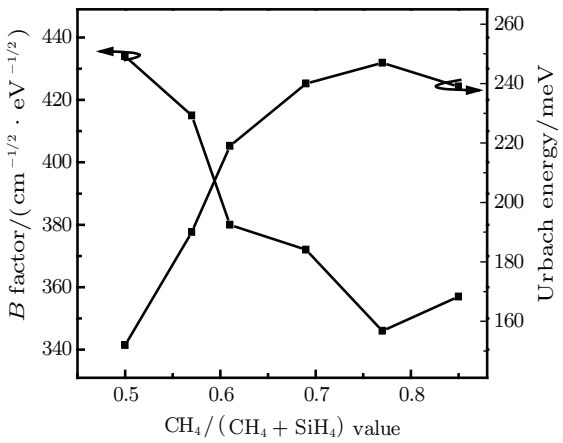


Fig. 5. Urbach energy and B factor of the film versus the $CH_4/(CH_4+SiH_4)$ ratio.

Room-temperature PL spectra of the films are reported in Fig. 6, where the excitation wavelength is 375 nm. The optical emissions can be controlled to change from near-infrared to visible by varying the film composition, and the PL peaks shift monotonically toward higher energy with the increase of carbon content. There are three main PL mechanisms in the optical emission of α-SiC:H films, which are related to defect states optical emission,[7] quantum confinement effect induced optical emission,[8,17] and band tail state optical emission,[4,7] respectively. For defect states-related PL, the PL peak position is fixed at a certain wavelength, which is not consistant with the blue shifting of the PL in our film. For a quantum confinement effect-induced PL, PL blue shifting occurs when the size of the nanoparticle becomes small, and the smaller nanoparticle in a high carbon content can be obtained by increasing the band gap. The PL blue shift with the increase of carbon content also occurs in band tail states-related optical emissions. As can be seen, the PL intensity increases with the increase of carbon content, and a maximal PL value is obtained in the S_5. The radiative recombination probability will be enhanced when the nanoparticles become small, and the maximal PL intensity should be obtained in the S_6 if the PL is caused by the quantum confinement effect, which is in discrepancy with the scenario in our films. In the band tail state PL model, the PL intensity is related to the activation energy of the carrier in the band tail. Room-temperature PL in amorphous silicon is quenched because thermal excitation can easily bring photon-generated carriers from the band tail state to the extended state, through which the carriers eventually recombine via nonradiative processes.[18] Adding carbon atoms to the film produces deeper states, which increase the activation energy of the carrier in the tail. As a result, thermal quenching is suppressed, and high intensity PL can be achieved at room temperature.[19] The disorder reduction in the C-riched film reduces the activation energy of the carrier in the band tail, which lowers the PL intensity again. The above results suggest that only the results obtained from the band tail state PL model is consistent with our PL results, and it will be confirmed further.

As can be seen in Fig. 7, there is a linear relationship between the Stocks shift of the PL and the $E_{\rm u}$ of the film. According to the static disorder model, the PL is caused by the radiative recombination of the photogenerated carriers in the exponential band tail. The radiative recombination happens only when the carriers reach the deepest states, and the PL Stokes shift is given by

$$E_{04} - E_{\rm PL} = \alpha E_{\rm u}, \tag{3}$$

where $E_{\rm PL}$ is the PL peak photon energy with the absorption coefficient α being 10^4 cm^{-1}.[20]

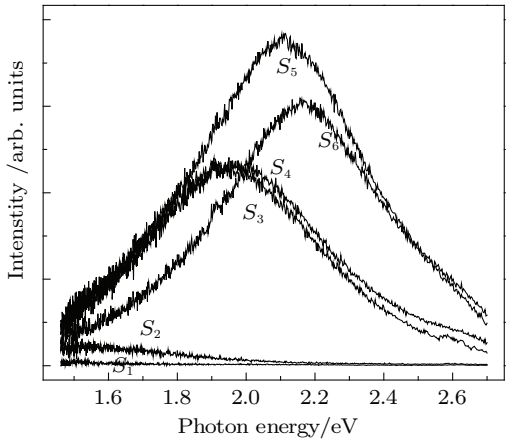


Fig. 6. The PL spectra of the films at different $CH_4/(CH_4+SiH_4)$ ratios.

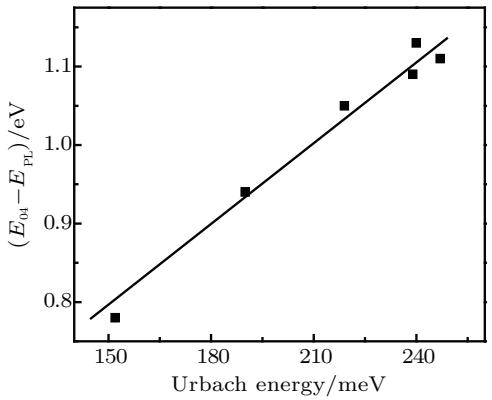


Fig. 7. Stocks shift versus $E_{\rm u}$ of the film.

Time-resolved PL spectra at different wavelengths are measured, and the results of S_5 are shown in Fig. 8. The PL decay times show a decreasing tendency at longer wavelengths. Curve fittings are performed at different wavelengths, and the fitting results at 600 nm are shown in the inset of Fig. 8. Three exponential decay processes are obtained, and the triple-exponential decay law suggests that multiple energy levels may be involved in the radiative recombination. Previous studies show that all the three decay processes

are related to a kind of band tail state in the band gap.[21] After the fast thermalization process in the band edge, the photon generated electrons and holes start a slower thermalization process in the band tail.

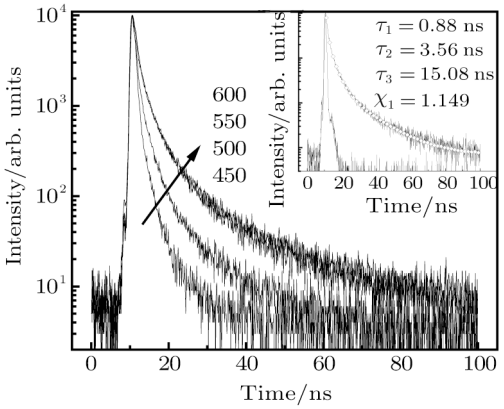


Fig. 8. PL decay curves at different wavelengths of S_5. The inset shows the curve fittings at 600 nm.

Radiative recombination happens when the carriers reach the deepest band tail state. The deeper the state, the longer time it needs for electron–hole pair recombination.[22] When the PL occurs between the band tail state of conduction and the valance band, the recombination through a deeper state gives a lower energy photon with a longer luminescence lifetime, and the slow decay components become larger and larger with a PL redshift appearing. The presence of broad tail states in the α-SiC:H film can well account for the dependence of the average lifetime on emission energy. As can be seen in Fig. 9, where

$$\bar{\tau} \propto \exp\left(-\frac{E_{\mathrm{m}}}{\gamma}\right). \tag{4}$$

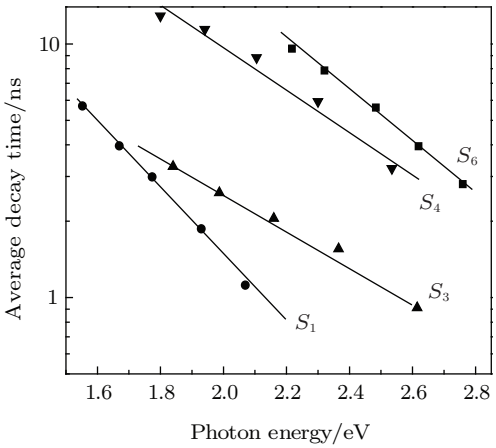


Fig. 9. Average decay times at different wavelengths for different films.

Such a dependence could be explained by the thermalization process through which photogenerated carriers stay in the lower-energy tail state. The thermalization rate is proportional to the density of band tail states that are involved in the processes. Thus, γ depends on the slope of the exponential band tail state density, and a sharper state density leads to a smaller γ.[20]

Consequently, the optical band gap, the PL peak position, the PL intensity, the Stock shift, and the average decay times of the films suggest that the optical emissions in our films are attributed to band tail luminescence.

4. Conclusion

The α-SiC:H films were deposited and a tunable room-temperature PL spectra from the near-infrared region to the visible region were obtained. The optical band gap of the film increases with the increase of the CH4 flow rate, while the disorder of the film increases monotonically until the film is near-stoichiometric. The relationship between PL peak energy, PL spectra width, and the optical band gap as well as the average decay times support that the optical emissions originate from optical transitions from the band tail state in the amorphous SiC matrix.

References

[1] Tran T N, SuendoV and Cabarroeas P R 2005 *Appl. Phys. Lett.* **87** 011903
[2] Imer A G, Yildiz I and Turan R 2010 *Physica* E **42** 2358
[3] Zhuo S Y, Liu X C, Ze X, Yan W S, Xin J, Yang J H and Shi E W 2012 *Chin. Phys.* B **21** 067503
[4] Cui J, Rusli, Yoon S F, Yu M B, Chew K, Ahn J, Zhang Q, Teo E J, Osipowicz T and Watt F 2001 *J. Appl. Phys.* **89** 2699
[5] Basa D K, Abbate G, Ambrosone G, Coscia U and Marino A 2010 *J. Appl. Phys.* **107** 023502
[6] Munekata H and Kukimoto H 1983 *Appl. Phys. Lett.* **42** 432
[7] Sreet R A, Nickel N H and Tsai C C 1995 *J. Non-Cryst. Solids* **190** 33
[8] Coscia U, Ambrosone G and Basa D K 2008 *J. Appl. Phys.* **103** 063507
[9] Kerdiles S, Berthelot A, Gourbilleau F and Rizk R 2000 *Appl. Phys. Lett.* **73** 7623
[10] Basa D K and Smith F W 1990 *Thin Solid Films* **192** 121
[11] Katiyar M, Yang Y H and Abelson J R 1995 *J. Appl. Phys.* **78** 1659
[12] Petrich M A, Gleason K K and Reimer J A 1987 *Phys. Rev.* B **36** 9722
[13] Rusli K C, Yoon S F, Ahn J, Ligatchev V, Teo E J, Osipowicz T and Watt F 2002 *J. Appl. Phys.* **92** 2937

[14] Karcher R, Ley L and Johnson R L 1984 *Phys. Rev.* B **30** 1896

[15] Yu W, Lu W B, Li H and Fu G S 2004 *J. Phys.* D: *Appl. Phys.* **37** 3304

[16] Chu V, Conde J P, Jarego J, Brogueira P, Rodriguez J, Barradas N and Soares J C 1995 *J. Appl. Phys.* **78** 3164

[17] Wang J Z, Suendo V, Abramov A, Yu L and Cabarrocas P R 2010 *Appl. Phys. Lett.* **97** 221113

[18] Street R A 1981 *Adv. Phys.* **30** 593

[19] Wang M, Xie M, Ferraioli L, Yuan Z, Li D, Yang D and Pavesi L 2008 *J. Appl. Phys.* **104** 083504

[20] Giorgis F, Vinegoni C and Pavesi L 2000 *Phys. Rev.* B **61** 469

[21] Fritzsche H 1994 *Appl. Phys. Lett.* **65** 2824

[22] Wakita K, Makimura S and Nakayama Y 1995 *Jpn. J. Appl. Phys.* Part 1 **34** 1425